Available online at www.sciencedirect.com
ScienceDirect
International Journal of Mass Spectrometry 260 (2007) 158–165
International Journal of Mass Spectrometry
www.elsevier.com/locate/ijms

MALDI-TOF and cluster-TOF-SIMS imaging of Fabry disease biomarkers

David Touboul [a], Sandrine Roy [b], Dominique P. Germain [c], Pierre Chaminade [b], Alain Brunelle [a], Olivier Laprévote [a,*]

[a] *Laboratoire de Spectrométrie de Masse, Institut de Chimie des Substances Naturelles (ICSN), CNRS, UPR 2301 Avenue de la Terrasse, 91198 Gif-sur-Yvette Cedex, France*
[b] *Groupe de Chimie Analytique E3343, Faculté de Pharmacie Paris XI, rue J.B. Clément, 92290 Châtenay-Malabry, France*
[c] *Assistance Publique-Hôpitaux de Paris, Paris, France*

Received 30 March 2006; received in revised form 21 September 2006; accepted 22 September 2006
Available online 2 November 2006

Abstract

Fabry disease is an X-linked disorder of glycosphingolipid metabolism, in which a partial or total deficiency of α-galactosidase A, a lysosomal enzyme, results in the progressive accumulation of neutral glycosphingolipids (globotriaosylceramide and digalactosylceramide) in most fluids and tissues of the body. Few information is available about the composition and distribution in tissues of the accumulated glycosphingolipids species. Mass spectrometry imaging is an innovative technique, which can provide pieces of information about the distribution of numerous biological compounds, such as lipids, directly on the tissue sections. MALDI-TOF and cluster-TOF-SIMS imaging approaches were used to study the localization of lipids (cholesterol, cholesterol sulfate, vitamin E, glycosphingolipids . . .) on skin and kidney sections of patients affected by the Fabry disease. Numerous information on pathophysiology were enlightened by both techniques.

Keywords: MALDI-TOF; Cluster-TOF-SIMS; Imaging mass spectrometry; Glycosphingolipid; Fabry disease

1. Introduction

Fabry disease (FD) is an X-linked inborn error of metabolism with severe clinical consequences. Affected patients have a deficiency of α-galactosidase A (α-Gal A), the lysosomal enzyme responsible for the breakdown of globotriaosylceramide (Gb_3) and digalactosylceramide (Ga_2) [1]. The deficiency of α-Gal A leads to the progressive accumulation of these two neutral glycosphingolipids (GSLs) in plasma and lysosomes of most cells in the body, among which various types of renal and cutaneous cells. GSLs, which are ubiquitous components of eukaryotic cell membranes, consist in a non-polar lipid (ceramide) portion acting as a membrane anchor and a hydrophilic carbohydrate moiety [2]. The structure of their glycosyl group defines the specific lipid class to which they belong. The ceramide skeleton is a long-chain sphingoid base which is substituted by a fatty acyl group. The molecular species differing by structural variations of the ceramide moiety constitute the micro-heterogeneity of the lipid class. These differences are related to the carbon chain length and to the degree and position of unsaturation and hydroxylation of both fatty acyl and sphingoid base structures.

Fabry disease can be diagnosed by a markedly deficient α-Gal A activity in males and by genetic studies in males and females [3]. Examination of biological samples such as urine or plasma, using detection or quantitation of Gb_3 and Ga_2 by high performance liquid chromatography (HPLC) and/or mass spectrometry [4–10] is the third diagnostic option, although false negative may occur in attenuated (“cardiac”) variants of the disease. Other approaches such as electron microscopy of tissue biopsies [1], allow the observation of enlarged lysosomes containing undegraded glycosphingolipids, but without any structural or quantitative information. In addition, electron microscopy experiments carried out on skin samples may lead to false negative results due to the patchy nature of the skin deposit in heterozygotes (female).

Two major imaging techniques can be used to analyze tissue sections by mass spectrometry. Matrix-assisted laser desorption/ionization (MALDI) [11,12] needs the sample surface to be coated with a matrix, and is generally used to map peptides and proteins [13,14]. Secondary ion mass spectrometry (SIMS)

* Corresponding author. Tel.: +33 1 69 82 30 32; fax: +33 1 69 07 72 47.
E-mail address: Olivier.Laprevote@icsn.cnrs-gif.fr (O. Laprévote).

1387-3806/$ – see front matter © 2006 Elsevier B.V. All rights reserved.
doi:10.1016/j.ijms.2006.09.027

[15,16] is a desorption/ionization method based on the ion emission after the impact on the surface of keV energy primary ions. Due to the low desorption efficiency of mono-atomic primary ion sources, the mass range for biological imaging is limited, without special sample preparation methods, to *m/z* ~200. With the development of polyatomic primary ion sources such as liquid metal ion sources [17], the secondary ion emission yields have been greatly improved [18–21] and the mass range available for imaging is now extended to more than 1000 Da. Moreover, for biological applications, cluster-SIMS does not need any tissue preparation, whereas the homogeneous matrix deposition by air-spray coating is difficult for MALDI. An alternative way to increase the sensitivity of SIMS without using cluster primary ions is to coat the sample with metals [22] and/or MALDI matrices [23,24], but this method, although efficient, keeps the disadvantage of the necessary homogeneous coating with also possible mass interferences.

MALDI and cluster-SIMS imaging mass spectrometry (IMS) techniques, fitted with time-of-flight (TOF) mass analyzers, both offer the unique possibility to analyze numerous compounds in mixture and to access to their distribution on thin tissue sections [25,26]. In MALDI-TOF the spatial resolution is usually about 25–50 μm, whereas for cluster-TOF-SIMS a spatial resolution of about 1 μm can be reached with the bismuth cluster ion source. A primary beam focus in the ~200 nm range can be obtained, but at the expense of the mass resolution, which is a prerequisite for accurate mass measurements and assignments.

The present work describes the application of these two IMS approaches for the characterization of glycosphingolipids accumulated in cutaneous and renal biopsies obtained from several hemizygote (male) patients affected with Fabry disease. The distribution of other lipids determined by cluster-TOF-SIMS imaging experiments also led to a better understanding of the biological processes underlying Fabry disease.

2. Material and methods

Cutaneous biopsies were obtained from adult and paediatric hemizygous (male) patients and from healthy volunteers. Renal biopsies were obtained after informed consent from two adult hemizygous patients. The samples were cooled to −160 °C in liquid nitrogen and stored at −80 °C. They were cut at a temperature of −20 °C and at a thickness of 20 μm, using a LEICA CM3050 S cryostat (Leica Microsystems SA, Rueil Malmaison, France). The section of the cutaneous biopsies included epidermis, dermis and hypodermis. For renal biopsies, the cortical (more external) and the medullar (more internal) parts were analyzed separately. The tissues sections were deposited on stainless steel plates (Goodfellow, Ermine Business Park, Huntingdon PE29 6WR, England) or on conductive glass slides [27] (Delta Technologies, Stillwater, MN, USA) for TOF-SIMS and MALDI-TOF analysis, respectively. No treatment was used for the TOF-SIMS experiments. For the MALDI experiments, after drying under a pressure of a few hPa for 15 min, the sections

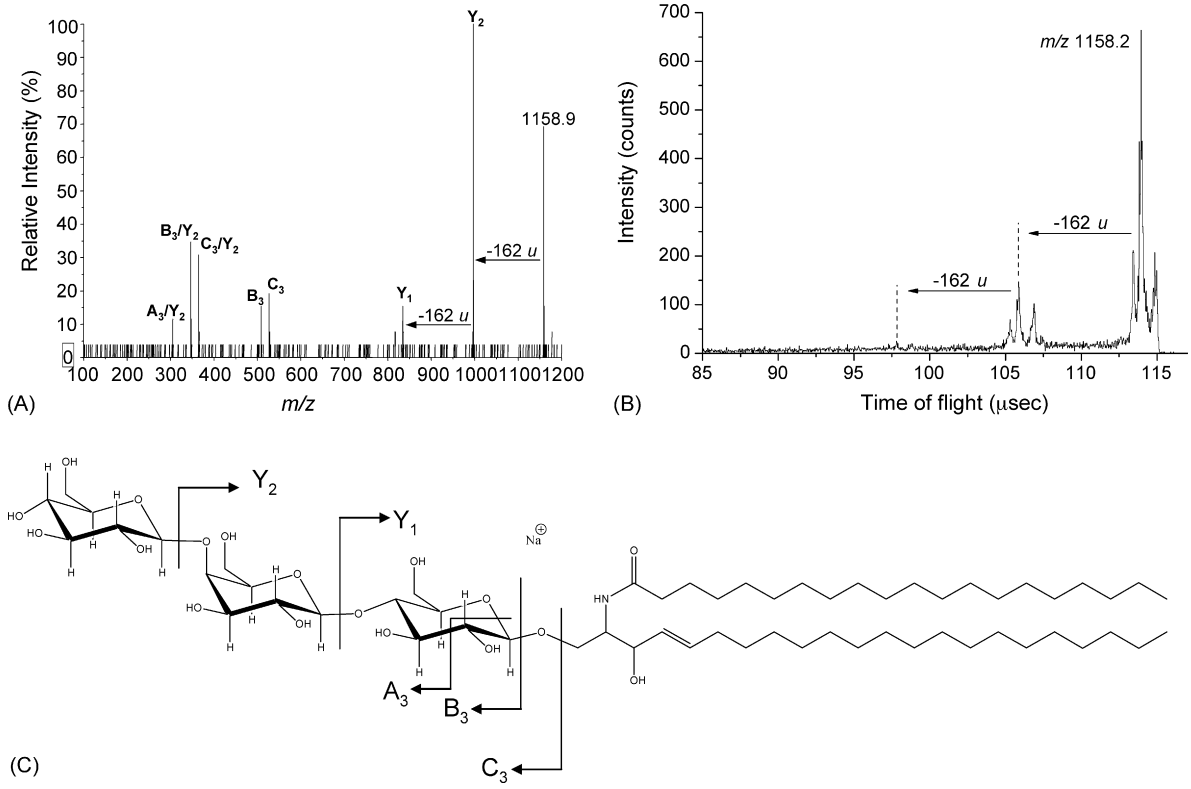

Fig. 1. (A) MALDI-MS/MS spectrum of the Gb_3 ion at *m/z* 1158.9 from a section of a Fabry patient skin biopsy. The fragment ions are labelled according to the nomenclature of Costello and Vath [50] further modified and expanded by Adams and Ann [51]. (B) Reflex TOF-SIMS fragment ion spectrum of the precursor ion at *m/z* 1158.9 in the positive ion mode, recorded at the surface of a Fabry patient kidney biopsy section. (C) Nomenclature for cleavages of neutral glycosphingolipids in positive ionisation mode illustrated with a globotriaosylceramide Gb_3.

were coated using an air-spray with the MALDI matrix solution [28] (α-cyano-4-hydroxycinnamic acid, purchased from Sigma–Aldrich, Saint-Quentin Fallavier, France, 20 mg mL^{-1} in acetone/methanol 50/50, v/v).

The TOF-SIMS imaging experiments were performed on a TOF-SIMS IV mass spectrometer (ION-TOF GmbH, Münster, Germany). The primary ion source was a liquid metal ion source with a bismuth cluster emitter which can deliver, in particular, Bi_3^+ ions. The kinetic energy of these ions was 25 keV, with an angle of incidence of 45°. The pulsed primary ion current was about 0.34 pA at 10 kHz, with a pulse duration of ∼1 ns when arriving on the sample. The secondary ions were accelerated to a kinetic energy of 2 keV and were post accelerated to 10 keV just before hitting a hybrid detector made of a single microchannel plate followed by a scintillator and a photomultiplier. The effective ion flight path was about 2 m (reflectron mode), allowing a mass resolution exceeding $M/\Delta M = 10^4$ (full width half maximum (FWHM)) at *m/z* 500. Because of the very low initial kinetic energy distribution of the secondary ions, the relationship between the time-of-flight and the square root of *m/z* is always linear over the whole mass range. Consequently, the internal mass calibration was made initially with H^+, H_2^+, and CH_3^+ ions in the positive ion mode and with H^-, C^-, CH^-, CH_2^-, C_2^- and C_2H^- ions in the negative ion mode. To further improve the mass accuracy and the mass assignment, the mass calibration was refined as previously described, using higher mass fragment ions [29]. All the images were recorded with a primary ion dose density (between 1.0 and 1.2 × 10^{12} ions cm^{-2}) below that of the static limit, i.e., 10^{13} ions cm^{-2}. To increase the contrast, the images were compressed to 128 × 128 pixels (final resolution, 3.9 μm) during the data processing and an averaging process can be applied. The name of the compounds or the *m/z* value of the peak centroïd, the maximal number of counts in a pixel (mc), and the total number of counts (tc) are shown below each image. The colour scales correspond to the interval [0, mc]. The reflex TOF-SIMS fragment ion spectrum from the precursor ion at *m/z* 1158.9 was acquired according to the method already described in ref. [30]. Briefly, a precursor ion is selected by two deflection plates. In flight, metastable decompositions occur in the field-free region of the TOF analyzer. Then, the difference of mass between the precursor ion and a fragment ion is proportional to their time-of-flight difference. In this case, no collision cell and no modification of the mass spectrometer is needed.

The MALDI-TOF imaging experiments were performed on a Voyager DE-STR mass spectrometer (Applied Biosystem, Les Ulis, France) equipped with a 20 Hz pulsed laser nitrogen (337 nm) and an electrostatic mirror. Mass spectra were acquired in the 500–2000 *m/z* range. The total acceleration voltage was set at 20 kV with a grid percentage of 65% and a delayed extraction time of 150 ns. External mass calibration was achieved using a

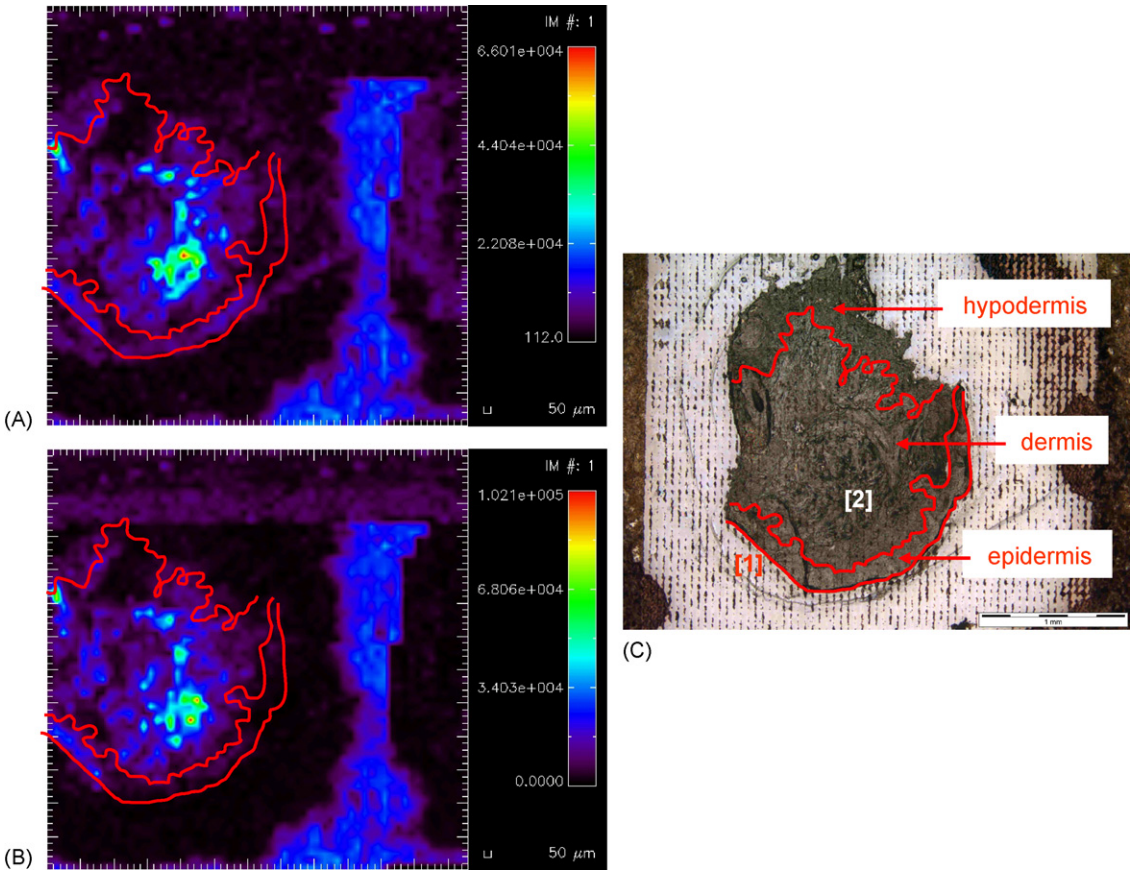

Fig. 2. (A and B) MALDI-TOF images of (A) the ion at *m/z* 1010.8 (Ga_2) and (B) the ion at *m/z* 1158.9 (Gb_3) acquired from a section of a Fabry patient skin biopsy. Image size 3.5 mm × 3.5 mm. (C) Optical image of the same tissue section after the MALDI-TOF images acquisition. The laser impacts are clearly visible outside of the section. Scale bar is 1 mm.

standard solution of Gb_3, purchased from Biovalley (Marne-la-Vallée, France). The images were recorded and processed using the IMT home-made software [31]. The number of laser shots per pixel was set to 50 and the spatial resolution was 50 μm.

MALDI-MS/MS experiments were performed on a quadruple/time-of-flight QStar Pulsar *i* tandem mass spectrometer (Applied Biosystems, Les Ulis, France) fitted with an o-MALDI source. The mass spectra were calibrated with the standard solution of Gb_3. The collision energy was set at 100 eV and nitrogen gas (N_2) was introduced in the collision cell so as to attain a pressure of about 10^{-2} Pa.

Reproducibility was ensured for all experiments by the study of several adjacent tissue sections.

3. Results and discussion

A standard Gb_3 solution was first analyzed by TOF-SIMS and MALDI-TOF. In both cases, the major species were sodium adduct ions $[M+Na]^+$. No in-source fragment was observed during MALDI-TOF experiments, whereas few low mass fragments signals were recorded in TOF-SIMS. In both cases, no sugar unit loss was detected.

For skin and kidney sections, chemical structures were confirmed by MALDI-MS/MS or PSD-TOF-SIMS experiments. Two examples are given in Fig. 1A and B. Due to the small size of the samples and to the relatively low sensitivity for these MS/MS experiments, only few fragments were detected. Nevertheless, losses of sugar units could be clearly observed, with strongly supports the peak assignments.

The first imaging experiments were carried out on sections of cutaneous biopsies from adult and paediatric hemizygous patients and from healthy volunteers. Fig. 2A and B display the MALDI images of two different glycosphingolipids at *m/z* 1010.7 and *m/z* 1158.9, corresponding to a Ga_2 with a ceramide skeleton C42:2-OH and a Gb_3 with a ceramide skeleton C42:1, respectively. The optical image of the skin section is provided in Fig. 2C. These MALDI-TOF images clearly demonstrate the possibility to obtain spatial distribution of a single glycosphingolipid molecular species by MALDI-TOF imaging. All the extracted maps display exactly the same accumulations in the dermis and hypodermis, whereas a weak glycosphingolipid signal was recorded in the epidermis. The specificity of the glycosphingolipid accumulation was confirmed by the absence of Ga_2 or Gb_3 signals in the mass spectrum recorded on the section obtained from the healthy volunteer cutaneous biopsy (Fig. 3C). The spectra extracted from different areas of the images shown in Fig. 2 are displayed in Fig. 3A and B.

The detected species and their relative intensities are very close to those observed on urinary extracts for the adult hemizygotes [8]. This may suggest that the structures of the accumulated species in Fabry disease could be identical for organs and biological fluids.

TOF-SIMS experiments on sections from cutaneous biopsies confirm the low amount of Ga_2 or Gb_3 in the epidermis. The cluster primary ion source made possible to acquire images of the global Ga_2 and Gb_3 signals on cutaneous biopsies sections (Fig. 4). Nevertheless, it was not possible to map one

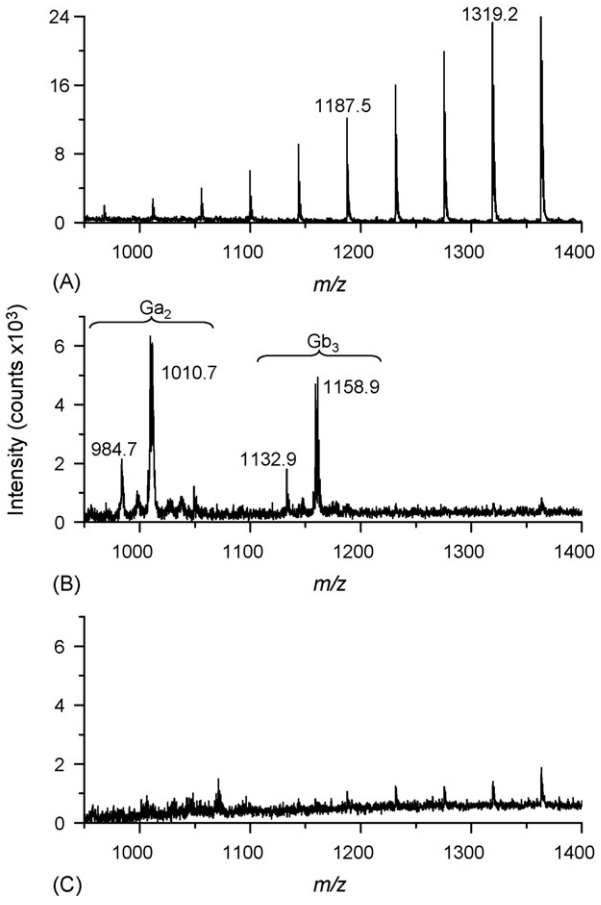

Fig. 3. (A) MALDI-TOF mass spectrum obtained at the edge of the skin biopsy section (area labelled [1] in Fig. 2C). The signal series between *m/z* 950 and *m/z* 1400 corresponds to the embedding glue. (B) MALDI-TOF mass spectrum obtained from the dermis part of a Fabry patient skin biopsy section (area labelled [2] in Fig. 2C). (C) MALDI-TOF mass spectrum obtained from a skin biopsy section of a healthy volunteer.

single glycosphingolipid compound with this technique. A control experiment confirmed the absence of GSLs signals on the sections from healthy volunteers' cutaneous biopsies. The spectrum extracted from the region rich in Ga_2 and Gb_3 (Fig. 5) displays a specific signal of the glycosphingolipids accumulated in Fabry disease but with a low signal-to-noise ratio compared to MALDI-TOF. It must also be noted that the accumulated species and their relative intensities are quite the same than for the prior MALDI-TOF experiments. This suggests that the recorded signal can be independent on the desorption/ionization method, which was confirmed by the analysis of the Gb_3 standard solution, also leading to the same profile for both techniques.

It was possible to record the distribution, on the cutaneous biopsy section, of other organic compounds, such as cholesterol, cholesterol sulfate and vitamin E. Cholesterol is characterized by the ions $[M+H-H_2O]^+$ at *m/z* 369.3 and $[M-H]^+$ at *m/z* 385.3 in the positive ion mode and a $[M-H]^-$ ion at *m/z* 385.3 in the negative ion mode [29]. Vitamin E ions are detected at *m/z* 430.4 ($[M]^{\bullet+}$) in the positive ion mode together with the fragment ions at *m/z* 165 and 205 [32]. In the negative ion mode,

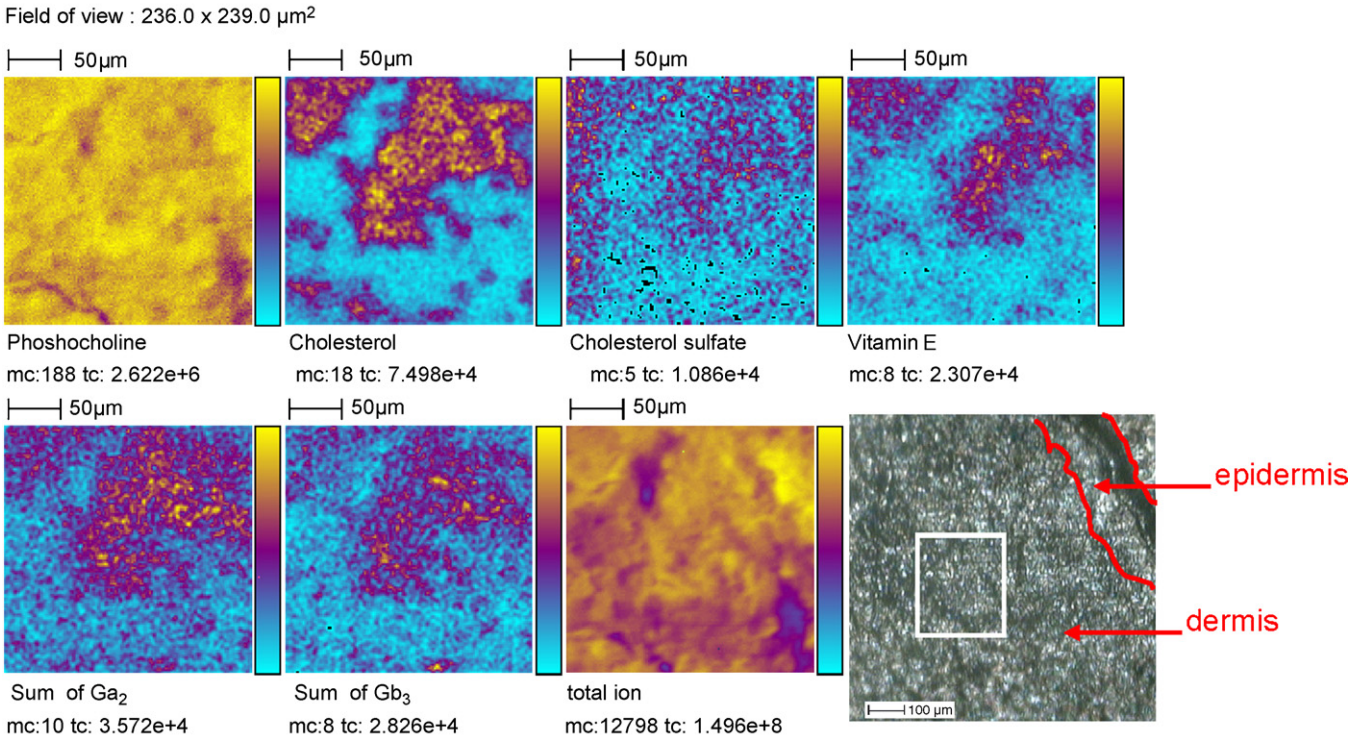

Fig. 4. Cluster-TOF-SIMS images of various molecules present in a Fabry patient skin biopsy section, deposited on a stainless steel plate without any treatment. Identification of compounds was made on the basis of diagnostic ions (see text). Field of view 236 μm × 236 μm. Pixel size ∼1 μm; Bi_3^+ projectiles; primary ion dose density, for each acquisition: 1.25×10^{12} ions cm^{-2}. mc corresponds to the maximal counts in one pixel and tc to the total counts in the image. The last image corresponds to the optical image, in which the analyzed area is delimited by the white square. The Ga_2 and Gb_3 images correspond to the selected *m/z* ranges 880–1030 and 1040–1200, respectively.

vitamin E leads to the deprotonated molecule $[M-H]^-$ at *m/z* 429.4. Cholesterol sulfate is characterized in the negative ion mode by the ion at *m/z* 465.4 ($[M-H]^-$) [33] which shows a loss of SO_3 under reflex TOF-SIMS conditions (data not shown). By contrast with the distributions of vitamin E, cholesterol, cholesterol sulfate and GSL, the ion at *m/z* 184 (phosphocholine) was shown to be homogeneously present on the tissue surface. The correlation between the molecular distributions will be further discussed in the article.

The second set of experiments was realized with renal biopsies. These samples were too small (∼200 μm) regarding to the laser spot size (∼50 μm) to acquire MALDI-TOF images. In that case, cluster-TOF-SIMS imaging proved to be an excellent alternative due to the focalization of the cluster ion beam at ∼1 μm. Clear accumulations of Ga_2 and Gb_3 were noted, in structures having a diameter of a few tens of micrometers, in both the cortical and medullar parts of a kidney biopsy from an adult hemizygous patient (for the medullar part, see Fig. 6). Although Ga_2 and Gb_3 are ubiquitous lipids of the organism, a signal increase can be correlated to the clinical evolution of Fabry disease. The clinical case examined in the present study corresponds to an end-stage renal disease [34]. Interestingly, the hydroxylated Gb_3 signals are more intense in the kidney than in the urinary sediment [8], whereas the Ga_2 profile is quite the same (Fig. 7).

The cluster-TOF-SIMS images of kidney biopsy sections, like those of skin biopsy sections, also revealed a colocalization of the intact Ga_2 and Gb_3 ions with vitamin E, cholesterol and cholesterol sulfate ions (Fig. 6).

Vitamin E is a generic denomination for tocopherols and tocotrienols. Only α-tocopherol was detected on skin and kidney biopsy sections by cluster-TOF-SIMS. Vitamin E is well-known for its antioxidant activity, preventing lipid peroxidation and other radical driven oxidative events. Due to its reductive power,

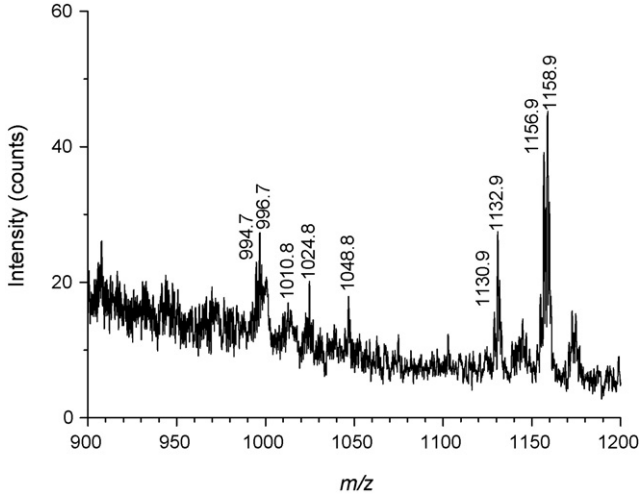

Fig. 5. Cluster-TOF-SIMS mass spectrum of the regions rich in Ga_2 and Gb_3 is observed, in the positive ion mode. The Ga_2 and Gb_3 ion peaks are observed in the *m/z* ranges 880–1030 and 1040–1200, respectively.

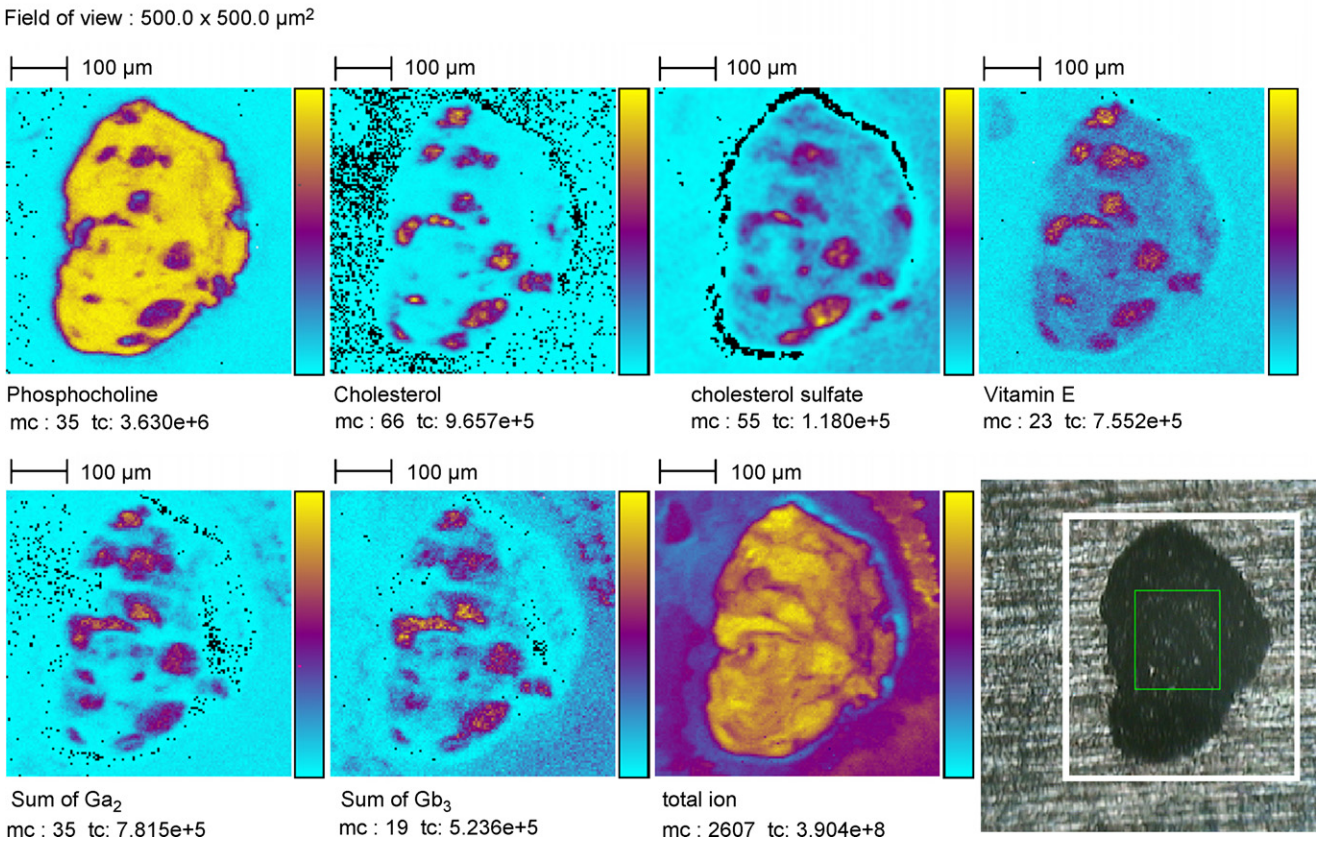

Fig. 6. Cluster-TOF-SIMS images of various molecules present in a Fabry patient kidney biopsy section deposited on a stainless steel plate without any treatment. Identification of compounds was made on the basis of diagnostic ions (see text). Field of view 500 µm × 500 µm. pixel size ~1 µm; Bi_3^+ projectiles; primary ion dose density, for each acquisition: 1.0×10^{12} ions cm^{-2}. mc corresponds to the maximal counts in one pixel and tc to the total counts in the image. The last image corresponds to the optical image, in which the analyzed area is delimited by the white square.

α-tocopherol can regulate the level of radical oxygen species ROS in a cell [35,36]. Therefore, the accumulation of vitamin E in a specific area of a tissue can be linked to a response against a local oxidative reaction [29]. Further, during an oxidative stress process, the level of nitric oxide ($NO^{\bullet}$) increases [36]. Then $NO^{\bullet}$ can react with the superoxide $O_2^{\bullet -}$, leading to the formation of peroxynitrite anions responsible for the nitration of tyrosine residues in proteins. In the case of Fabry disease, the enhanced nitrotyrosine immunohistochemical staining of the cerebral and dermal vasculature relative to control subjects [37], the ascorbate decrease of Fabry cerebral hyperfusion [38] and the reduction of the activity of respiratory chain enzymes [39] suggest ROS production abnormalities and accumulation. Moreover, a study showed a relationship between endothelial NO synthase gene variants and renal complications in hemizygotes affected with FD [40]. Finally, the level of α-tocopherol in plasma is lower for Fabry hemizygotes than for control subjects [41]. This could be explained by an increase of vitamin E incorporation in membrane cell, leading to a decreased level in plasma. It must be noted that it is the first time that an accumulation of an antioxidant molecule, vitamin E, was observed directly on tissue sections from Fabry patients' biopsies. Moreover, the cluster-TOF-SIMS images allowed to localize precisely α-tocopherol in areas where Ga_2 and Gb_3 are also accumulated.

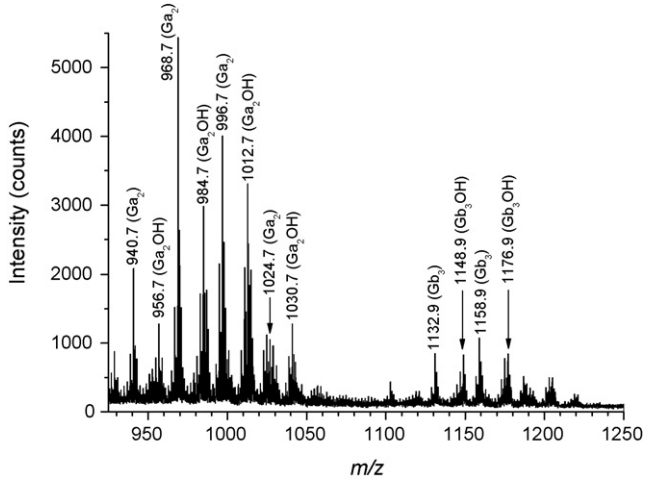

Fig. 7. Cluster-TOF-SIMS mass spectrum of the regions rich in Ga_2 and Gb_3 is observed, in the positive ion mode. The Ga_2 and Gb_3 ion peaks are observed in the *m/z* ranges 880–1030 and 1040–1200. The Ga_2(OH) and Gb_3(OH) labels stand for hydroxylated Ga_2 and Gb_3 species, respectively.

The colocalization of cholesterol and glycosphingolipids Ga_2 and Gb_3 is an other interesting point of the present study. Recently, a BODIPY-LacCer (fluorescent labelled lactosyl ceramide, LacCer) pulse-labelling of normal human skin fibroblasts showed a fluorescent signal in the Golgi complex,

while the LacCer is located in punctuate endocytic structures in fibroblasts isolated from Fabry patients [42,43]. Such an unusual intracellular localization of LacCer was shown to be linked to high cholesterol levels, which can lead to a deregulation of the membrane lipids and proteins traffic [44–46]. These results were only obtained on skin fibroblast cultures. For the first time, cluster-TOF-SIMS images enable to display the same localization of the cholesterol with Ga_2 and Gb_3, directly on skin and kidney sections from Fabry patient biopsies (Figs. 4 and 6), and thus confirm the prior results.

Finally, accumulations of cholesterol sulfate in skin and kidney biopsies of Fabry patients were clearly observed. Although this has never been reported before, some hypothesis can be formulated. In skin, cholesterol sulfate is known to be predominantly located in the epidermis. It is related to the formation of the epidermal barrier and in the process of keratinocyte differentiation [47,48]. Occurring during childhood or adolescence, the angiokeratomas are among the first symptoms of Fabry disease [49], and are small hyperkeratotic areas of dilated blood vessels. The excess of cholesterol sulfate could possibly be related to the skin modifications occurring in FD.

4. Conclusion

Cluster-TOF-SIMS and MALDI-TOF mass spectrometry imaging techniques have proved here to be interesting alternatives to conventional histochemistry analysis. Both Ga_2 and Gb_3 composition and repartition at a micrometer scale can be obtained directly on biopsy sections, together with those of other lipids such as cholesterol, cholesterol sulfate and vitamin E. These new innovative techniques could be also very useful to monitor the Ga_2 and Gb_3 clearance during an enzyme replacement therapy. Mass spectrometry revealed to be an efficient and robust tool for lipid imaging on tissue section, thus providing invaluable information for the diagnosis of genetic diseases.

Acknowledgement

D.T. is indebted to the Institut de Chimie des Substances Naturelles (CNRS) for a Ph.D. research fellowship.

References

[1] R.J. Desnick, R. Brady, J. Barranger, A.J. Collins, D.P. Germain, M. Goldman, G. Grabowski, S. Packman, W.R. Wilcox, Ann. Intern. Med. 138 (2003) 338.
[2] I.M. Morrisson, in: J.F. Kennedy (Ed.), Carbohydrate Chemistry, Oxford University Press, New York, 1988, p. 196.
[3] D.P. Germain, J. Shabbeer, S. Cotigny, R.J. Desnick, Mol. Med. 8 (2002) 306.
[4] W.J. Cable, R.H. McCluer, E.H. Kolodny, M.D. Ullman, Neurology 32 (1982) 1139.
[5] K. Mills, A. Johnson, B. Winchester, FEBS Lett. 515 (2002) 171.
[6] G. Fauler, G.N. Rechberger, D. Devrnja, W. Erwa, B. Plecko, P. Kotanko, F. Breunig, E. Paschke, Rapid Commun. Mass Spectrom. 19 (2005) 1499.
[7] V. Hunnam, D.J. Harvey, D.A. Priestman, R.H. Bateman, R.S. Bordoli, R. Tyldesley, J. Am. Soc. Mass Spectrom. 12 (2001) 1220.
[8] D. Touboul, S. Roy, D.P. Germain, A. Baillet, F. Brion, P. Prognon, P. Chaminade, O. Laprévote, Anal. Bioanal. Chem. 382 (2005) 1209.
[9] T. Kitagawa, N. Ishige, K. Suzuki, M. Owada, T. Ohashi, M. Kobayashi, Y. Eto, A. Tanaka, K. Mills, B. Winchester, J. Keutzer, Mol. Genet. Metab. 85 (2005) 196.
[10] F. Boscaro, G. Pieraccini, G. la Marca, G. Bartolucci, C. Luceri, F. Luceri, G. Moneti, Rapid Commun. Mass Spectrom. 16 (2002) 1507.
[11] M. Karas, D. Bachmann, U. Bahr, F. Hillenkamp, Int. J. Mass Spectrom. Ion Processes 78 (1987) 53.
[12] K. Tanaka, H. Waki, Y. Ido, S. Akita, Y. Yoshida, T. Yoshida, Rapid Commun. Mass Spectrom. 2 (1988) 151.
[13] R.M. Caprioli, T.B. Farmer, J. Gile, Anal. Chem. 69 (1997) 4751.
[14] M. Stoeckli, P. Chaurand, D.E. Hallahan, R.M. Caprioli, Nat. Med. 7 (2001) 493.
[15] R. Castaing, G. Slodzian, J. Microsc. 1 (1962) 395.
[16] A. Benninghoven, E. Loebach, Rev. Sci. Instrum. 42 (1971) 49.
[17] M. Benguerba, A. Brunelle, S. Della-Negra, J. Depauw, H. Joret, Y. Le Beyec, M.G. Blain, E.A. Schweikert, G. Ben Assayag, P. Sudraud, Nucl. Instrum. Methods Phys. Res. B 62 (1991) 8.
[18] D. Weibel, S. Wong, N. Lockyer, P. Blenkinsopp, R. Hill, J.C. Vickerman, Anal. Chem. 75 (2003) 1754.
[19] D. Touboul, F. Halgand, A. Brunelle, R. Kersting, E. Tallarek, B. Hagenhoff, O. Laprévote, Anal. Chem. 76 (2004) 1550.
[20] P. Sjövall, J. Lausmaa, B.L. Johansson, M. Andersson, Anal. Chem. 76 (2004) 1857.
[21] D. Touboul, F. Kollmer, E. Niehuis, A. Brunelle, O. Laprévote, J. Am. Soc. Mass Spectrom. 16 (2005) 1608.
[22] A.F. Maarten Altelaar, I. Klinkert, K. Jalink, R.P.J. de Lange, R.A.H. Adan, R.M.A. Heeren, S.R. Piersma, Anal. Chem. 78 (2006) 734.
[23] A.F. Maarten Altelaar, J. van Minnen, C.R. Jiménez, R.M.A. Heeren, S.R. Piersma, Anal. Chem. 77 (2005) 735.
[24] L.A. McDonnell, S.R. Piersma, A.F. Maarten Altelaar, T.H. Mize, S.F. Luxembourg, P.D.E.M. Verhaert, J. van Minnen, R.M.A. Heeren, J. Mass Spectrom. 40 (2005) 160.
[25] P.J. Todd, T.G. Schaaff, P. Chaurand, R.M. Caprioli, J. Mass Spectrom. 36 (2001) 355.
[26] A. Brunelle, D. Touboul, O. Laprévote, J. Mass Spectrom. 40 (2005) 985.
[27] P. Chaurand, S.A. Schwartz, D. Billheimer, B.J. Xu, A. Crecelius, R.M. Caprioli, Anal. Chem. 76 (2004) 1145.
[28] S.A. Schwartz, M.L. Reyzer, R.M. Caprioli, J. Mass Spectrom. 38 (2003) 699.
[29] D. Touboul, A. Brunelle, F. Halgand, S. De La Porte, O. Laprévote, J. Lipid Res. 46 (2005) 1388.
[30] D. Touboul, A. Brunelle, O. Laprévote, Rapid Commun. Mass Spectrom. 20 (2006) 703.
[31] IMT, Logiciel de traitement et d'analyse d'images par spectrométrie de masse, registered by CNRS and the French Agency for Software Protection, Paris, IDDN.FR.001.300028.000.S.P.2005.000.21000.
[32] E.B. Monroe, J.C. Jurchen, J. Lee, S.S. Rubakhin, J.V. Sweedler, J. Am. Chem. Soc. 127 (2005) 12152.
[33] S. Ghardashkhani, M.L. Gustavsson, M.E. Breiner, G. Larson, B.E. Samuelson, Rapid Commun. Mass Spectrom. 9 (1995) 491.
[34] M. Branton, R. Schiffmann, J.B. Kopp, J. Am. Soc. Nephrol. 13 (2002) S139.
[35] A.M. Miles, D.S. Bohle, P.A. Glassbrenner, B. Hansert, D.A. Wink, M.B. Grisham, J. Biol. Chem. 271 (1996) 40.
[36] V. Darley-Usmar, H. Wiseman, B. Halliwell, FEBS Lett. 369 (1995) 131.
[37] D.F. Moore, L.T. Scott, M.T. Gladwin, G. Altarescu, C. Kaneski, K. Suzuki, M. Pease-Fye, R. Ferri, R.O. Brady, P. Herscovitch, R. Schiffmann, Circulation 104 (2001) 1506.
[38] D.F. Moore, F. Ye, M.L. Brennan, S. Gupta, B.A. Barshop, R.D. Steiner, W.J. Rhead, R.O. Brady, S.L. Hazen, R. Schiffmann, J. Magn. Reson. Imaging 20 (2004) 674.
[39] T. Lucke, W. Hoppner, E. Schmidt, S. Illsinger, A.M. Das, Mol. Genet. Metab. 82 (2004) 93.
[40] C. Heltianu, G. Costache, A. Gafencu, M. Diaconu, M. Bodeanu, C. Cristea, K. Azibi, L. Poenaru, M. Simionescu, J. Cell Mol. Med. 9 (2005) 135.
[41] H. Sakuraba, T. Igarashi, T. Shibata, Y. Suzuki, Clin. Genet. 31 (1987) 349.

[42] C.S. Chen, M.C. Patterson, C.L. Wheatley, J.F. O'Brien, R.E. Pagano, Lancet 354 (1999) 901.
[43] A. Choudhury, M. Dominguez, V. Puri, D.K. Sharma, K. Narita, C.L. Wheatley, D.L. Marks, R.E. Pagano, J. Clin. Invest. 10 (2002) 1541.
[44] V. Puri, R. Watanabe, M. Dominguez, X. Sun, C.L. Wheatley, D.L. Marks, R.E. Pagano, Nat. Cell. Biol. 1 (1999) 386.
[45] K. Simons, J. Gruenberg, Trends Cell. Biol. 10 (2000) 459.
[46] D.J. Sillence, V. Puri, D.L. Marks, T.D. Butters, R.A. Dwek, R.E. Pagano, F.M. Platt, J. Lipid Res. 43 (2002) 1837.
[47] C.A. Strott, Y. Higashi, J. Lipid Res. 44 (2003) 1268.
[48] T. Kuroki, T. Ikuta, M. Kashiwagi, S. Kawabe, M. Ohba, N. Huh, K. Mizuno, S. Ohno, E. Yamada, K. Chida, Mutat. Res. 462 (2000) 189.
[49] A. Mehta, R. Ricci, U. Widmer, F. Dehout, A. Garcia de Lorenzo, C. Kampmann, A. Linhart, G. Sunder-Plassmann, M. Ries, M. Beck, Eur. J. Clin. Invest. 34 (2004) 236.
[50] C.E. Costello, J.E. Vath, Methods Enzymol. 193 (1990) 738.
[51] Q. Ann, J. Adams, Anal. Chem. 65 (1993) 7.